BIOCELL
2012, 36(3): 133-142

ISSN 0327 - 9545
PRINTED IN ARGENTINA

Structural analysis of flagellar axonemes from inner arm dynein knockdown strains of *Trypanosoma brucei*

RANDI ZUKAS[1], ALEX J. CHANG[1], MARIAN RICE[2], AMY L. SPRINGER[1*]

1. Department of Biology, Amherst College, Amherst, MA, USA
2. Department of Biological Sciences, Mount Holyoke College, South Hadley, MA, USA

Key words: Flagellar motility, transmission electron microscopy, central pair

ABSTRACT: *Trypanosoma brucei* is a protozoan flagellate that causes African sleeping sickness. Flagellar function in this organism is critical for life cycle progression and pathogenesis, however the regulation of flagellar motility is not well understood. The flagellar axoneme produces a complex beat through the precisely coordinated firing of many proteins, including multiple dynein motors. These motors are found in the inner arm and outer arm complexes. We are studying one of the inner arm dynein motors in the *T. brucei* flagellum: dynein-f. RNAi knockdown of genes for two components of dynein-f: DNAH10, the α heavy chain, and IC138, an intermediate chain, cause severe motility defects including immotility. To determine if motility defects result from structural disruption of the axoneme, we used two different flagellar preparations to carefully examine axoneme structure in these strains using transmission electron microscopy (TEM). Our analysis showed that inner arm dynein size, axoneme structural integrity and fixed central pair orientation are not significantly different in either knockdown culture when compared to control cultures. These results support the idea that immotility in knockdowns affecting DNAH10 or IC138 results from loss of dynein-f function rather than from obvious structural defects in the axoneme.

Introduction

Trypanosoma brucei is a protozoan flagellate that causes African sleeping sickness in humans and chronic wasting disease in sheep and cattle (Garcia *et al.,* 2006). Current treatments for these diseases have many drawbacks and at present there is great need for new drugs (Steverding, 2010). The *T. brucei* flagellum is critical for motility, cell morphogenesis, polarity, sensing and cell division (Gull, 2003; Ralston *et al.,* 2009; Rodríguez *et al.,* 2009), thus this organelle is a potential target for anti-trypanosomal compounds. The *T. brucei* flagellum consists of a cylindrical "9+2" arrangement of nine doublet microtubules encircling a pair of singlet microtubules. This arrangement is highly conserved among eukaryotic flagella (Ralston and Hill, 2008). Cell motility results from flagellar bending caused by dynein-driven sliding of doublet microtubules against one another (Porter and Sale, 2000). Dyneins are arranged in repeating units along the inner and outer face of the axoneme and are referred to as the inner and outer arms, respectively. Dyneins are complexes of several polypeptides, the largest of which are the heavy chains (HC) that contain motor domains (Gennerich and Vale, 2009). In the green alga *Chlamydomonas reinhardtii*, the inner and outer arms are thought to have different roles in flagellar movement: outer arm dyneins (OAD) prima-

*Address correspondence to: Amy L. Springer.
Department of Biology, Amherst College, Amherst, MA, USA.
E-mail: aspringer@amherst.edu
Received: June 14, 2012. Revised version received: October 6, 2012. Accepted: October 10, 2012.

rily generate force (Ishikawa *et al.,* 2007), and inner arm dyneins (IAD) determine the size and shape of the flagellar bend (Kotani *et al.,* 2007). Overall, production of a flagellar beat requires a precise coordination of all dyneins in the axoneme (Wirschell *et al.,* 2007; Lindemann and Lesich, 2010).

Despite the observed structural conservation of the axoneme, the *T. brucei* flagellum has some unique features, such as its attachment along the cell body, the presence of a paraflagellar rod (PFR) that runs along its length (Bastin *et al.,* 1996) and the tip-to-base bihelical beat (Ralston *et al.,* 2009; Rodríguez *et al.,* 2009). Furthermore, previous studies have suggested differences in roles of orthologous dynein components between *T. brucei* and *C. reinhardtii* or other eukaryotic flagella (Ralston *et al.,* 2006; Baron *et al.* 2007a). While comparisons of these components between organisms are helpful for understanding trypanosome flagellar structure, the functions of axonemal components may vary and for this reason *T. brucei* flagellar components should be studied specifically.

Dynein-f, is an IAD thought to play an important role in regulating flagellar waveform (Kotani *et al.,* 2007). We previously reported that silencing of the dynein-f α-HC gene (*dnah10*) in insect-stage *T. brucei* cells caused flagellar immotility as well as growth, cell division and morphological defects (Springer *et al.,* 2011), but did not see any structural changes by electron microscopy. To extend this analysis, we compared two different axonemal preparation processes using strains with RNAi knockdown of *dnah10* or of the gene for another dynein-f component, *ic138*. Flagellar preparations showed no significant differences in size of IAD, axonemal integrity or central pair orientation for either RNAi knockdowns or for either preparation method. This thorough TEM analysis demonstrates that the immotility phenotype is not a result of major structural defects and is more likely caused by the loss of dynein-f function after knockdown, suggesting that IAD function is critical for flagellar movement in trypanosomes.

Materials and Methods

Culturing and induction

T. brucei DNAH10^{RNAi} has been described previously (Springer *et al.,* 2011). IC138 ^{RNAi} was constructed in the same manner: a portion from nucleotides 453-868 of *Tbic138* (Tb927.2.4060; 5' primer: GATGTTGTTCCAATTCCATCC, 3' primer: TCCACGGTGTGACTTGTAACC), was amplified by PCR and ligated into *Hind*III and *Xho*I sites of pZJM (Wang *et al*., 2000). This construct was stably transfected into the 29-13 strain (Wirtz *et al.,* 1999), grown in SDM-79 medium (Brun and Schönenberger, 1979), and clonal lines were established as described (Chandler *et al.,* 2008). To induce RNAi, tetracycline was added to 1 μg/ml 48 hours prior to harvesting, and growth was monitored by hemacytometer. RNA isolation and real-time RT-PCR analyses were carried out as described (Springer *et al.* 2011) using the following *ic138* primers. Primer set 1: 5'primer: TTGCCT TTTCCGACGAGCAT, 3' primer: CCCATTTCAG CTCCCACACC, product size 156 bp. Primer set 2: 5'primer: CAGTGGCGTGGATGTTTTCG, 3' primer: AGACCTGACGTTGCCGCTTC, product size 163 bp.

Time-lapse motility assay

Log phase cultures were harvested and split to 1×10^6 cells/mL and incubated at room temperature for one hour. 10μL of cell culture was added to a poly-L-glutamate-coated slide chamber (Gadelha *et al.,* 2005), sealed with vaseline around the coverslip. Time-lapse images were generated by compiling 30 sequential images at 1 second intervals using a Nikon Eclipse E400 (nikon.com) under 20X objective, and outfitted with Spot Insight QE software (SPOT Imaging Solutions, diaginc.com). In general, dark field produced the best results for minimizing background and optimizing contrast of the cells, but every slide required special adjustments to optimize the image. Images were made black and white and the threshold was adjusted to recognize cells against the background. The compiled images were converted into motility traces with the Computer Assisted Sperm Analyzer (CASA) plug-in (Wilson-Leedy and Ingermann, 2007) for ImageJ (Abramoff *et al.,* 2004), run with the following parameters: minimum sperm size 20 pixels, maximum sperm size 1500 pixels, minimum track-length 2 frames, VSL, VAP and VCL all set to zero, and 30 frames per second. Occasionally, the minimum track-length was modified to produce more fluid traces of moving cells. After analysis, each trace was verified for accuracy using the original image before being classified as runner (cells with progressive movement for at least 5 seconds), tumbler (cells with flagellar beating, but no progressive movement), or immotile (cells with no net movement or flagellar beat) as described (Springer *et al.,* 2011).

Flagellar preparation

Flagellar preparation using the one-step extraction protocol has been described (Robinson *et al.,* 1991; Oberholzer *et al.,* 2009). Comparisons are made to flagella prepared previously from the two-step protocol (Springer *et al.* 2011). Approximately 2 x 10^8 cells were used for DNAH10^{RNAi} preparations, and 1.5 x 10^7 cells for IC138 ^{RNAi} preparations.

Transmission electron microscopy

Extracted flagella were prepared as described (Springer *et al.* 2011), and images were viewed on a Philips CM100 transmission electron microscope (FEI.com), captured digitally or scanned from Kodak Electron microscope film no. 4489 (Aremac.com).

Scoring axoneme images

IAD structures were counted and scored by size as described previously (Springer *et al.,* 2011). An axoneme was considered "broken" if it had no central pair, had a severely deformed shape, or if the circumference of microtubules was disrupted. Central pair (CP) orientation was assessed as described (Ralston *et al.,* 2006). Briefly, axoneme images in which the central pair was clearly discernible were selected randomly. A reference line was drawn from the center point of doublet 1 to that of doublet 7. A second line was drawn that bisected the central pair microtubules. The acute angle of intersection between these two lines was measured. The median angle was taken from the angles of all uninduced preparations, and the deflection from the median was recorded for each axoneme in the sample. Contrast and brightness adjustments were made in Adobe Photoshop CS3 (adobe.com) to increase IAD visibility. The IAD color density was not taken into account when making these assessments, since it was not possible to distinguish between differences due to variation in IAD size or to unequal stain distribution.

Results

The gene Tb927.2.4060 encodes the predicted ortholog to intermediate chain IC138 (Wickstead and Gull, 2007), and was silenced using tetracycline-inducible RNAi as described in Materials and Methods. Knockdown of *ic138* mRNA was confirmed by real time PCR analysis: by 48 hours post-induction the transcript levels were reduced to 27% of that seen in uninduced cultures (Fig. 1A). To monitor the effect of this knock-

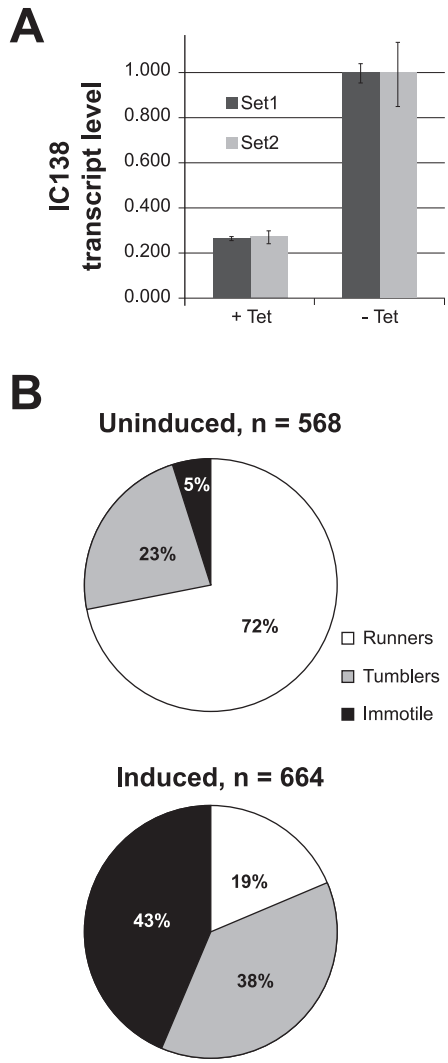

FIGURE 1. Analyses of IC138 ^{RNAi} knockdown cells.
A. Relative transcript levels of *ic138* RNA by real time RT-PCR analysis. Gene expression was normalized to the housekeeping genes *gapdh* and *rps23*. The level of gene expression in uninduced cells (-Tet) was set as 1.0, and the relative expression in tetracycline-induced IC138^{RNAi} cells (+Tet), from each of two different primer sets, is shown (Primer Set1, 0.268; Primer Set2, 0.277). Data represent averages from two independent sets of uninduced and induced cultures with standard deviations indicated by error bars.
B. Summaries of traces from time-lapse motility assays on IC138^{RNAi}. Pie charts with percentages of cells scored as runners (white), tumblers (gray) or immotile (black) in cultures that were either uninduced (above), or induced with tetracycline and grown 48 hours before analysis (below). Above each chart, the n represents the raw number of cells scored for each culture condition.

down, a motility assay was used to characterize the movement of individual cells from cultures in which RNAi was induced or uninduced. Motility traces were recorded using time-lapse microscopy (Fig. 1B) in which individual trypanosomes were observed for thirty seconds and classified as runner, tumbler or immotile as described in Materials and Methods. When compared to uninduced cells, induced IC138^{RNAi} showed a significant decrease in the percentage of runners, and an increase in percentages of both tumblers and immotile cells. By 48 hours post-induction, the immotile category is the largest at 43%, and only 5% of cells are runners.

In order to thoroughly assess the effect of *dnah10* or *ic138* knockdown on axoneme structure, we used the one-step preparation (Oberholzer *et al.,* 2009). The one-step method yields more complete axoneme structures, unlike the two-step method which removes OAD and structures in the axoneme center but leaves inner arms intact and more clearly discernible (Fig. 2). DNAH10^{RNAi} and IC138^{RNAi} cultures were induced for 48 hours, a time point at which a large percentage of IC138^{RNAi} cells (Fig. 1), and a distinct majority of DNAH10^{RNAi} cells (Springer *et al.,* 2011) are immotile.

Flagellar fractions were always prepared simultaneously on RNAi-induced cultures and uninduced cultures that had been cultured in parallel. Flagella were prepared from both IC138^{RNAi} and DNAH10^{RNAi} strains; for the latter, two preparations were completed independently. The resulting images were compared to images of DNAH10^{RNAi} from a two-step preparation described previously (Springer *et al.,* 2011). All axoneme preparations were scored for number of IAD by size (Fig. 3) and results are shown in Table 1. To assess whether the RNAi knockdown led to any overall loss of structural integrity, the fraction of broken axonemes relative to intact axonemes was measured from each sample set (Table 1). For both criteria, there were no significant differences between samples in which RNAi had been induced and the corresponding uninduced samples, as determined by Chi-square analysis.

The CP microtubules maintain a fixed orientation in the *T. brucei* axoneme relative to extra-axonemal structures such as the PFR (Ralston *et al.,* 2006; Branche *et al.,* 2006). Because the one-step method leaves the PFR–axoneme intact in most cases, these preparations provide a better opportunity for scoring CP orientation relative to PFR orientation. At least 25 axonemes were

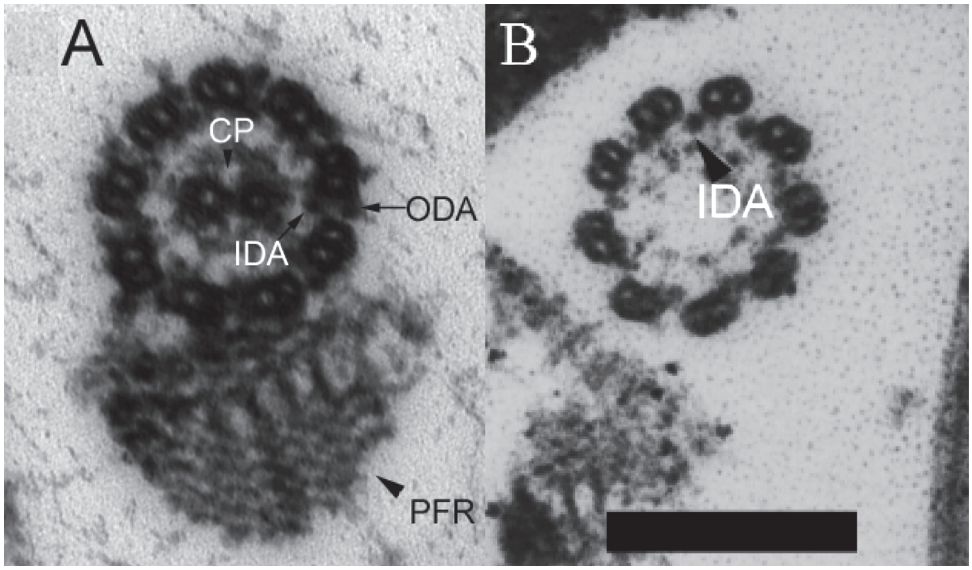

FIGURE 2. Representative axoneme images from one-step (A) and two-step (B) preparations. Both preparations remove flagellar membranes but axonemes from the one-step preparation retain the OAD, radial spoke and central pair structures. Axonemes from the two-step preparation have lost these structures, yielding an unobstructed view of the IAD structures. In the two-step preparation, the PFR in often missing or broken as shown here, this is likely due to residual protease activity (possibly contaminating the DNase reaction), not to the salt extraction per se (Oberholzer *et al.*, 2009). Scale bar is 200 nm.

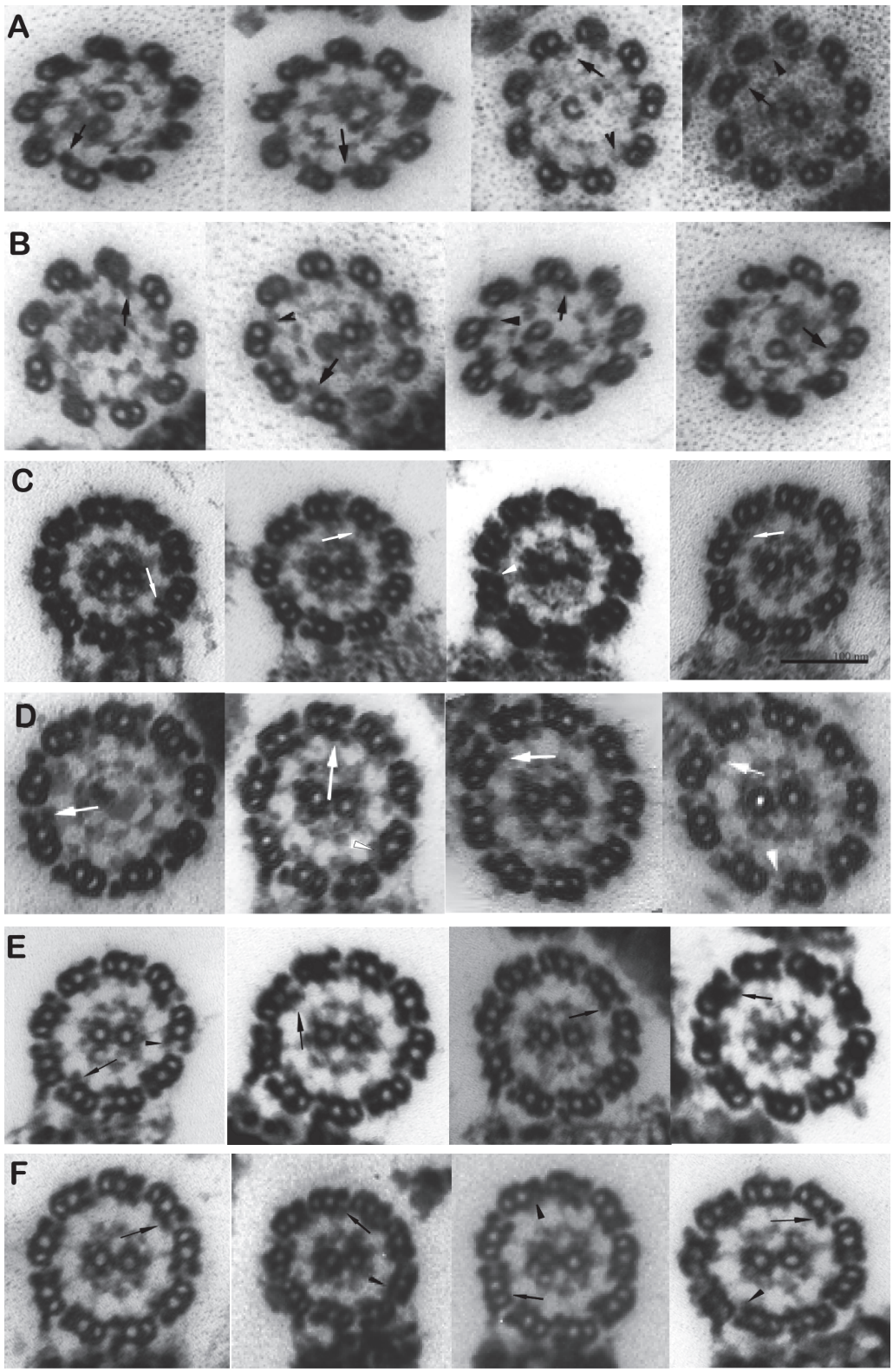

FIGURE 3. Representative axonemes from various preparations. Uninduced and RNAi-induced samples were prepared for TEM using the one-step preparation or two-step preparation. Four representative film images of individual axonemes are shown for each preparation. (A,B) Two-step preparation of DNAH10^{RNAi} uninduced and knockdown induced samples, respectively. (C,D) One-step preparation of DNAH10^{RNAi} uninduced and induced samples, respectively. (E,F) One-step preparation of IC138^{RNAi} uninduced and induced samples, respectively. An example of an IAD scored as intact or large is shown with an arrow, an IAD scored as small is shown with an arrowhead. Scale bar is 100 nm.

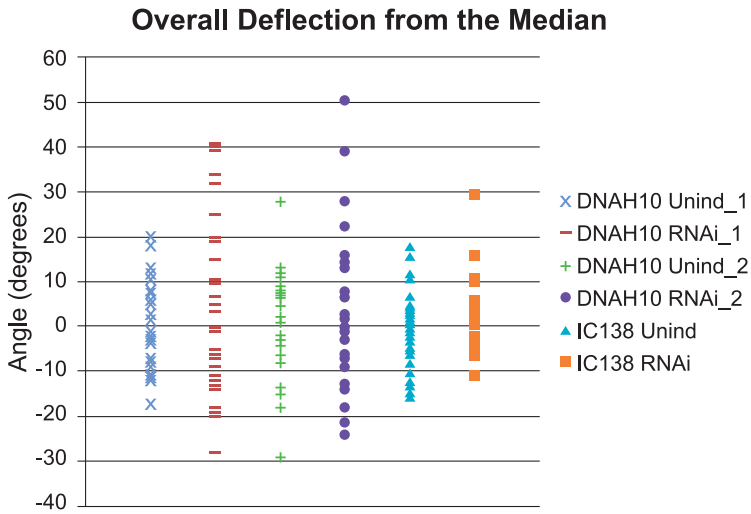

FIGURE 4. Distribution of central pair orientation angles deflected from the median angle of 61 degrees. A dot plot representing the deflection of the central pair-PFR angle from the median for each individual axoneme is shown for each preparation. Nomenclature for labeling of axoneme preparations is described for Table 1.

TABLE 1.

Summary of inner arm dynein size and axoneme integrity analysis[a]

Sample		IAD size/axoneme, mean values[b]						IAD integrity				
		Large	Small	Ratio	n	p-value	Comparison	Intact	Broken	n	Fraction	p-value
Two-step[c]	DNAH10, uninduced	8	1	0.13	81			755	259	1014	0.26	
	DNAH10, RNAi	7.8	1.2	0.15	54	0.266	RNAi to Unind.[d]	250	78	328	0.24	0.522
One-step	DNAH10-1, uninduced	8.31	0.69	0.08	16			99	31	130	0.24	
	DNAH10-1, RNAi	7.95	1.05	0.13	19	0.084	RNAi to Unind.	135	31	166	0.19	0.278
	DNAH10-2, uninduced	8.53	0.47	0.06	15			130	35	165	0.21	
	DNAH10-2, RNAi	8.15	0.85	0.10	20	0.159	RNAi to Unind.	120	31	151	0.21	0.882
	Comb. DNAH10 uninduced	8.42	0.58	0.07	31	0.071	1-step to 2-step[e]	229	66	295	0.22	0.267
	Comb. DNAH10 RNAi	8.05	0.95	0.12	39	0.395	DNAH10 to IC138[f]	255	62	317	0.20	0.073
	IC138, uninduced	8.35	0.65	0.08	40			256	83	339	0.24	
	IC138, RNAi	8.26	0.74	0.09	24	0.694	RNAi to Unind.	303	102	405	0.25	0.826
	Total uninduced	8.38	0.62	0.07	71			485	149	634	0.24	

[a]Nomenclature for Table 1, Table 2 and Figure 3: the label "DNAH10" represents the DNAH10^{RNAi} strain, and "IC138" represents the IC138 ^{RNAi} strain, either with RNAi induced or uninduced, as indicated. "-1" and "-2" refer to independent flagellar preparations with the same strain and conditions.

[b] Total number large + small IAD/axoneme is always 9.0

[c]From (Springer *et al.* 2011).

[d]Comparison between RNAi-induced and uninduced preparations of the same *T. brucei* strain

[e]Comparison between DNAH10^{RNAi}, uninduced from one-step preparation and DNAH10^{RNAi}, uninduced from two-step preparation

[f]Comparison between RNAi-induced DNAH10^{RNAi} strains and RNAi-induced IC138^{RNAi} strain

TABLE 2.

Summary of central pair orientation analysis[a]

Sample	Median angle	Mean deflection	n	P-values for deflections[b]	
				Wilcoxon RS	Kolmogorov-Smirnoff
DNAH10-1, uninduced	62.0º	1.19º	29		
DNAH10-1, RNAi	59.3º	4.72º	30	0.791	0.404
DNAH10-2, uninduced	56.5º	1.52º	25		
DNAH10-2, RNAi	61.5º	1.02º	28	0.476	0.675
IC138, uninduced	61.0º	-0.45º	41		
IC138, RNAi	58.3º	3.19º	26	0.153	0.375
Total uninduced samples	61.0º	0.56º	95		

[a] Summary of median angles and mean deflections measured from each preparation. N = number of axonemes measured.
[b]Wilcoxon RS = the Wilcoxon Rank Sum test, Kolmogorov-Smirnov = the Kolmogorov-Smirnov test. These tests were performed by comparing the measured deflections from the respective RNAi-induced preparation to the measured deflections from total uninduced sample set. The α level for statistical significance was 0.05.

scored from each RNAi induced and uninduced preparation. An overall median angle of 61º was determined from all measurements of uninduced samples from either strain. For each axoneme, the CP angle was measured and the deflection from the median angle was recorded (Fig. 4 and Table 2). It appeared that the range of angles might have been greater in the RNAi-induced samples relative to the respective uninduced samples. In order to test this statistically, we employed two statistical tests: The Wilcoxon rank sum test (Wild and Seber, 1999) the Kolmogorov-Smirnov test for two-independent samples (Daniel, 2000). These do not require normal distributions, since our sample sizes were small and not all datasets generated normal distributions. For each preparation we compared the measured deflections from the median for each RNAi-induced preparation, to those from the total uninduced sample set, using $P<0.05$ as the α level of statistical significance. In both tests, the differences in range of deflection values were not significant between induced and uninduced samples.

Discussion

We have presented a structural analysis of axonemes from *T. brucei* strains in which *dnah10* or *ic138* has been knocked down. Extensive TEM analysis of axoneme images, comparing the one-step (less stringent) preparation to the two-step (more stringent) preparation, shows that no gross structural defects are evident in these strains that show a severe motility defect. These results are consistent with the interpretation that immotility in these strains is a consequence of the loss of function of the targeted dynein-f components, perhaps including the loss of other associated axonemal proteins. This suggests that proper IAD function is necessary for motility.

It was not surprising that the knockdown of a single HC such as DNAH10 did not cause a visible change in size by TEM: IAD structures are massive, containing 6-8 HCs, thus the loss of one HC is a relatively minor change in the overall IAD electron density (Kamiya *et al.,* 1991). In addition to IAD size, we assessed axonemal integrity and CP orientation since this structure in *T. brucei* maintains a fixed orientation. While dynein-f is not expected to interact with CP directly, the protein complexes that transduce the CP signal lie near the base of the dynein-f complex (Lindemann and Lesich, 2010) and loss of DNAH10 or IC138 could prevent the assembly of multiple proteins. Indeed in *C. reinhardtii*, loss of DNAH10 or IC138 has been shown to affect the assembly of other proteins (Myster *et al.,* 1997; Bower *et al.,* 2009). It is possible that loss of either of these proteins could destabilize a complex that helps in some way to maintain the CP orientation. This orientation can be more effectively examined in the one-step preparation since the CP and PFR are more intact. Our results suggest that the RNAi-induced strain might yield a greater range in CP angles, but this difference in range

was shown not to be statistically significant using two different non-parametric tests. While it is possible that the extent of the knockdown in each culture might affect this result, overall we see no significant disruption in CP orientation in these strains. Although we see no structural disruption of axonemes in these strains, we still believe that TbDNAH10 and TbIC138 are flagellar proteins. Both proteins were predicted to be orthologs of known flagellar proteins based on comprehensive phylogenetic analysis (Wickstead and Gull, 2007) and both proteins have been identified as components of flagella in independent proteomic and genomic analyses of *T. brucei* flagella (Broadhead *et al.,* 2006; Baron *et al.,* 2007b). Because axonemal components have been highly conserved during evolution (Holzbaur and Vallee, 1994), these orthologs can be reasonably assumed to form equivalent structures in different organisms. Therefore we are confident that these proteins reside in the *T. brucei* flagellum.

In *C. reinhardtii*, DNAH10 is thought to play an important role in regulating flagellar waveform (Kotani *et al.,* 2007); it exhibits slower gliding velocities than other dynein HCs and is oriented in a more oblique angle relative to the microtubule than other inner arm HCs (Bui *et al.,* 2008). *C. reinhardtii* dynein-f is thought to inhibit the extent of sliding of adjacent microtubules and modulate the amount of curvature of the flagellar bend (Kotani *et al.,* 2007). *C. reinhardtii* IC138 is a regulatory protein, inhibited by phosphorylation and thought to negatively regulate DNAH10 (Wirschell *et al.,* 2007). Because of these roles, knockdown of either of these proteins might reasonably be expected to interfere with normal coordination of dynein movement in flagellar bending, and our results suggest that a complete inner arm is necessary for flagellar beating in *T. brucei.* Further analyses of these strains will extend our understanding of their roles in regulating bending in the *T. brucei* flagellum.

This study presents an approach that could be generally useful to assess integrity and quality of axoneme structure using TEM in flagellar mutants. Our analysis provides evidence that the immotility in *dnah10* and *ic138* knockdowns results from disrupting coordination of flagellar movement not overall flagellar structure.

Acknowledgements

We thank Sue Lancelle for assistance with sample preparation, Sulynn Machado for assistance with culturing, Amherst College Biology Department for support, and Dr. Shu-Min Liao for statistical consulting.

References

Abramoff MD, Magalhães PJ, Ram SJ (2004). Image processing with ImageJ. *Biophotonics International* **11**: 36–42.

Baron DM, Kabututu ZP, Hill KL (2007a). Stuck in reverse: loss of LC1 in *Trypanosoma brucei* disrupts outer dynein arms and leads to reverse flagellar beat and backward movement. *Journal of Cell Science* **120**: 1513–1520.

Baron DM, Ralston KS, Kabututu ZP, Hill KL (2007b). Functional genomics in *Trypanosoma brucei* identifies evolutionarily conserved components of motile flagella. *Journal of Cell Science* **120**: 478–491.

Bastin P, Matthews KR, Gull K (1996). The paraflagellar rod of kinetoplastida: solved and unsolved questions. *Parasitology Today* **12**: 302–307.

Bower R, VanderWaal K, O'Toole E, *et al.* (2009) IC138 defines a subdomain at the base of the I1 dynein that regulates microtubule sliding and flagellar motility. *Molecular Biology of the Cell* **20**: 3055–3063.

Branche C, Kohl L, Toutirais G, Buisson, J, Cosson J, Bastin P (2006) Conserved and specific functions of axoneme components in trypanosome motility. *Journal of Cell Science* **119**: 3443–3455.

Broadhead R, Dawe HR, Farr H, Griffiths S, Hart SR, Portman N, Shaw MK, Ginger ML, Gaskell SJ, McKean PG, Gull K (2006) Flagellar motility is required for the viability of the bloodstream trypanosome. *Nature* **440**: 224–227.

Brun R, Schönenberger, M (1979) Cultivation and *in vitro* cloning of procyclic culture forms of *Trypanosoma brucei* in a semi-defined medium. *Acta Tropica* **36**: 289–292.

Bui KH, Sakakibara H, Movassagh T, Oiwa K, Ishikawa T (2008) Molecular architecture of inner dynein arms *in situ* in *Chlamydomonas reinhardtii* flagella. *Journal of Cell Biology* **183:** 923–932.

Chandler J, Vandoros AV, Mozeleski B, Klingbeil MM (2008) Stem-loop silencing reveals that a third mitochondrial DNA polymerase, POLID, is required for kinetoplast DNA replication in trypanosomes. *Eukaryotic Cell* **7**: 2141–2146.

Daniel WW (2000) *Applied Nonparametric Statistics*. Duxbury Press, Pacific Grove, CA.

Gadelha C, Wickstead B, de Souza W, Gull K, Cunha-e-Silva N (2005) Cryptic paraflagellar rod in endosymbiont-containing kinetoplastid protozoa. *Eukaryotic Cell* **4**: 516–525.

Garcia A, Courtin D, Solano P, Koffi M, Jamonneau V (2006) Human African trypanosomiasis: connecting parasite and host genetics. *Trends in Parasitology* **22**: 405–409.

Gennerich A, Vale RD (2009) Walking the walk: how kinesin and dynein coordinate their steps. *Current Opinion in Cell Biology* **21**: 59–67.

Gull K (2003) Host-parasite interactions and trypanosome morphogenesis: a flagellar pocketful of goodies. *Current Opinion in Microbiology* **6**: 365–370.

Holzbaur ELF, Vallee RB (1994) Dyneins: Molecular Structure and Cellular Function. *Annual Review of Cell Biology* **10**: 339–372.

Ishikawa T, Sakakibara H, Oiwa K (2007) The architecture of outer dynein arms in situ. *Journal of Molecular Biology* **368**: 1249–1258.

Kamiya R, Kurimoto E, Muto E (1991) Two types of *Chlamydomonas* flagellar mutants missing different components of inner-arm dynein. *The Journal of Cell Biology* **112 :** 441–447.

Kotani N, Sakakibara H, Burgess SA, Kojima H, Oiwa K (2007) Mechanical properties of inner-arm dynein-f (dynein I1)

studied with *in vitro* motility assays. *Biophysical Journal* **93**: 886–894.

Lindemann CB, Lesich KA (2010) Flagellar and ciliary beating: the proven and the possible. *Journal of Cell Science* **123**: 519–528.

Myster SH, Knott JA, O'Toole E, Porter ME (1997) The *Chlamydomonas* Dhc1 gene encodes a dynein heavy chain subunit required for assembly of the I1 inner arm complex. *Molecular Biology of the Cell* **8**: 607–620.

Oberholzer M, Lopez MA, Ralston KS, Hill KL (2009) Approaches for functional analysis of flagellar proteins in African trypanosomes. *Methods in Cell Biology* **93**: 21–57.

Porter ME, Sale WS (2000) The 9 + 2 axoneme anchors multiple inner arm dyneins and a network of kinases and phosphatases that control motility. *Journal of Cell Biology* **151**: F37–42.

Ralston KS, Hill KL (2008) The flagellum of *Trypanosoma brucei*: new tricks from an old dog. *International Journal for Parasitology* **38**: 869–884.

Ralston KS, Kabututu ZP, Melehani JH, Oberholzer M, Hill KL (2009) The *Trypanosoma brucei* flagellum: moving parasites in new directions. *Annual Review of Microbiology* **63**: 335–362.

Ralston KS, Lerner AG, Diener DR, Hill KL (2006) Flagellar motility contributes to cytokinesis in *Trypanosoma brucei* and is modulated by an evolutionarily conserved dynein regulatory system. *Eukaryotic Cell* **5**: 696–711.

Robinson D, Beattie P, Sherwin T, Gull K (1991) Microtubules, tubulin, and microtubule-associated proteins of trypanosomes. *Methods in Enzymology* **196**: 285–299.

Rodríguez JA, Lopez MA, Thayer MC, Zhao Y, Oberholzer M, Chang DD, Kisalu NK, Penichet ML, Helguera G, Bruinsma, R, Hill KL, Miao J (2009) Propulsion of African trypanosomes is driven by bihelical waves with alternating chirality separated by kinks. *Proceedings of the National Academy of Sciences (USA)* **106**: 19322–19327.

Springer AL, Bruhn DF, Kinzel KW, Rosenthal NF, Zukas R, Klingbeil MM (2011) Silencing of a putative inner arm dynein heavy chain results in flagellar immotility in *Trypanosoma brucei*. *Molecular and Biochemical Parasitology* **175**: 68–75.

Steverding D (2010) The development of drugs for treatment of sleeping sickness: a historical review. *Parasites & Vectors* **3**: 15.

Wickstead B, Gull K (2007) Dyneins across eukaryotes: a comparative genomic analysis. *Traffic* **8**: 1708–1721.

Wild CJ, Seber GAF (1999) *Chance Encounters: A First Course in Data Analysis and Inference*. John Wiley, New York.

Wilson-Leedy JG, Ingermann RL (2007) Development of a novel CASA system based on open source software for characterization of zebrafish sperm motility parameters. *Theriogenology* **67**: 661–672.

Wirschell M, Hendrickson T, Sale WS (2007) Keeping an eye on I1: I1 dynein as a model for flagellar dynein assembly and regulation. *Cell Motility and the Cytoskeleton* **64**: 569–579.

Wirtz E, Leal S, Ochatt C, Cross GA (1999) A tightly regulated inducible expression system for conditional gene knock-outs and dominant-negative genetics in *Trypanosoma brucei*. *Molecular and Biochemical Parasitology* **99**: 89–101.